Reaction Sintering of Cold-Extruded Elemental Powder Mixture Ti-48Al

G.-X. WANG and M. DAHMS

The influence of the extrusion ratio on sintering behavior of cold-extruded powder mixture Ti-48Al has been investigated. Both pressureless reaction sintering and hot isostatic pressing (HIP) without encapsulation were carried out. Moreover, two-step sintering, *i.e.*, combination of pressureless sintering and HIP, was conducted. It was found that both porosity and pore size in reactively sintered specimens largely decrease with increaseing extrusion ratio. For a given extrusion ratio, the porosity after pressureless sintering decreases with increasing temperature. Although a reduction of porosity can be reached by directly HIP specimens, the effect of applied pressure in case of combined treatments is strongly dependent on extrusion ratio. By applying an extremely high extrusion ratio of 350, material with a porosity of only 0.7 pct has been prepared by pressureless sintering and subsequent HIP without encapsulation while a reverse treatment route led to a porosity of 5%. On the contrary, lower porosities were obtained for low extrusion ratios of 17 and 25 by HIP and following pressureless sintering. The effect of extrusion ratio, as well as sintering temperature, was discussed. In addition, pore coalescing, gas penetration, and swelling were considered in order to understand the effect of applying pressure.

I. INTRODUCTION

TITANIUM aluminide alloys based on the intermetallic compound TiAl have become more interesting owing to their potential applications as high-temperature materials. These alloys exhibit low densities, high melting temperatures, good mechanical properties, and environmental resistance at elevated temperatures. They are mostly produced using ingot metallurgy. However, earlier work has shown that it is possible to prepare TiAl-based alloys by reactive powder metallurgy (RPM).[1,2] In the RPM processing, the cold-extrusion technique is used to consolidate the elemental Ti- and Al-powder mixtures with or without additives. The as-extruded material exhibits no intermetallics and can therefore be easily machined to complex shapes, which are then reactively sintered to get the desired intermetallics. In this way, the poor workability of titanium aluminides can be evaded. During reaction sintering, more Al atoms move into Ti particles and lead to formation of pores if no pressure is applied. The final pore size is proportional to the size of Al regions. Normally, hot isostatic pressing (HIP) is applied to compress pores. An HIP treatment requires encapsulation of extruded pieces due to their open porosity and is therefore relatively expensive. It is thus of practical importance to reduce the size of Al regions and the open porosity of extruded pieces. This can be achieved by increasing the extrusion ratio φ, which is defined as the area ratio of the specimen cross sections before (A_1) and after extrusion (A_2). In this study, we report on the influence of the extrusion ratio φ on pore formation in Ti-48Al during both pressureless reaction sintering and HIP without encapsulation. Two-step sintering, *i.e.*, combination of pressureless sintering and HIP, was also conducted.

G.-X. WANG and M. DAHMS are with the Institute for Materials Research, GKSS Research Centre, 21502 Geesthacht, Germany.

Manuscript submitted October 2, 1992.

II. EXPERIMENTAL

Elemental titanium and aluminium powders of sizes smaller than 100 μm, with purities of 99.8 pct and 99.9 pct, respectively, were mixed in air to the desired composition Ti-48 at. pct Al. The powder mixture was uniaxially pressed at room temperature with 500 MPa to a green compact. This compact was cold extruded (at room temperature) using different extrusion ratios of φ = 17 and 25. A considerably higher extrusion ratio was obtained by bundling pieces of a previously extruded rod (Mueller *et al.*[3]) and by extruding the bundle again to give a total extrusion ratio of 350. Altogether, three extrusion ratios were applied in this study: φ = 17, 25, and 350.

The extruded specimens were reactively sintered under different conditions: in a vacuum ($\approx 10^{-3}$ N/m^2) furnace for 6 hours at 600 °C, 1000 °C, and 1350 °C and in HIP equipment at 1350 °C/4 h/200 MPa. A heating rate of 20 °C/min was used in both cases. A combination of both pressureless sintering and HIP, *i.e.*, first pressureless sintering and then HIP or vice versa, was also conducted.

As-extruded specimens as well as specimens reactively sintered under different conditions were examined using light microscopy (LM). A quantative determination of the porosity, as well as the pore size distribution in the reactively sintered specimens, was carried out with the help of a computer-aided image analysis system. Polarized light was used to observe microstructural details, such as grain and phase boundaries. X-ray difraction analysis was carried out to get information about phase formation.

III. RESULTS

A. *Characterization of As-Extruded Conditions*

Figure 1 shows the microstructures of the three as-extruded conditions with Al having a light and Ti a dark

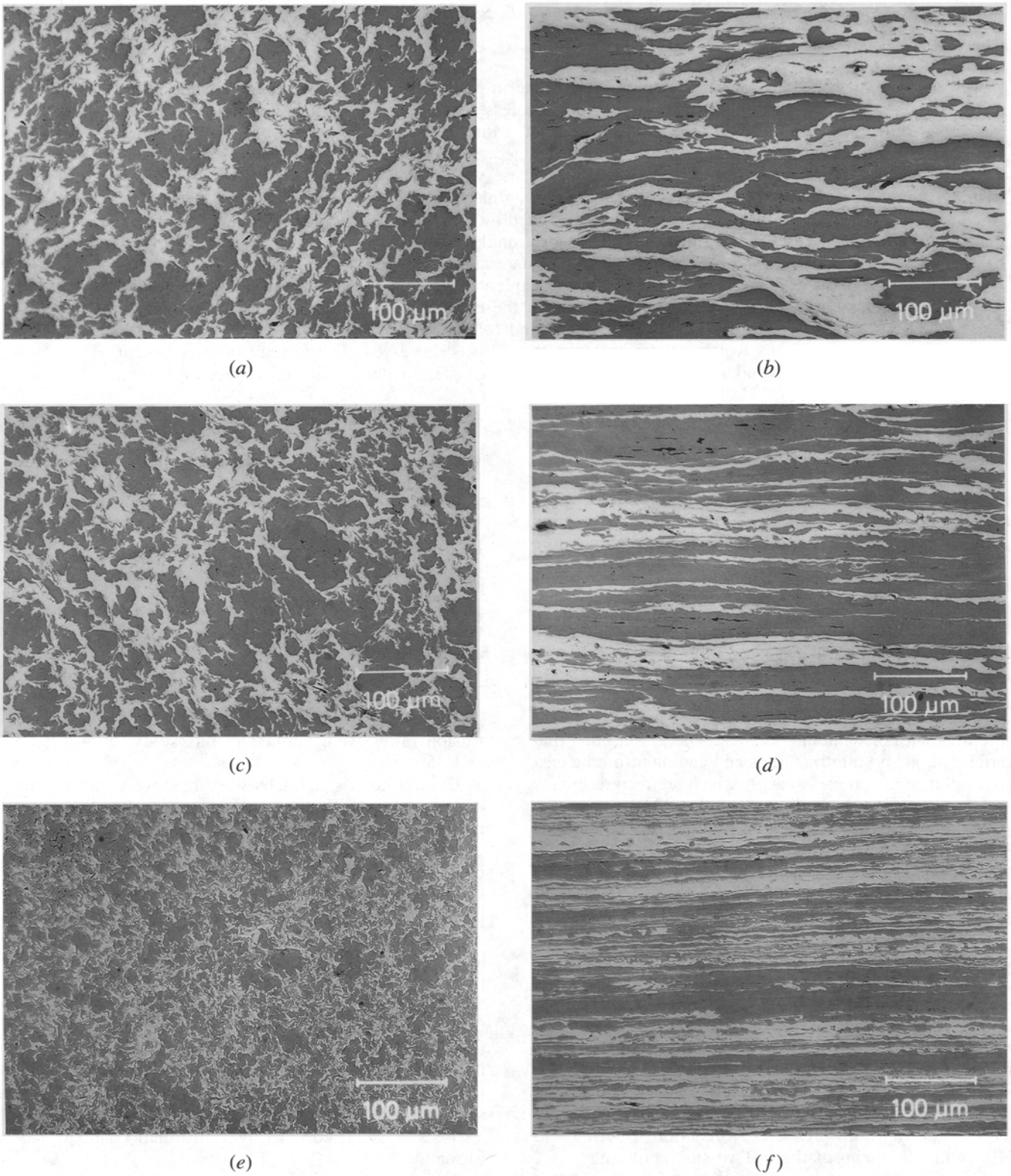

Fig. 1—LM photographs of as-extruded conditions with extrusion ratio of (*a*) and (*b*) 17, (*c*) and (*d*) 25, and (*e*) and (*f*) 350 in directions (a), (c), and (e) perpendicular and (b), (d), and (f) parallel to the extrusion direction.

appearance. During extrusion, particles, especially the Al particles, are elongated in the extrusion direction to fibers. With increasing extrusion ratio, both Al and Ti fibers become thinner and longer. Some small pores, mostly situated between Ti particles, can be detected in the specimens extruded with the low extrusion ratios of 17 and 25 (Figures 1(a) through (d)). The porosity is smaller than 0.5 pct. The specimen with the high extrusion ratio of 350 exhibits almost no pores (Figures 1(e) and (f)).

During extrusion with high extrusion ratios, a local temperature increase, which can cause reaction between elemental Ti and Al to the intermetallic phases, is possible due to heavy deformation. However, as shown in Figure 2, only intensity peaks of pure Ti and Al were measured by X-ray difraction analysis. It can thus be concluded within detection limits of about 5 vol pct that the reaction of elemental Ti and Al to intermetallics did not take place during extrusion, even with an extrusion ratio as high as 350. The as-extruded materials therefore can be easily machined or reformed to diffrent shapes. This is, as pointed out earlier, of practical importance, since the presence of titanium aluminides will make the manufacture much more difficult. The as-extruded materials are strongly textured because of the alignment of both Al and Ti fibers in extrusion direction (Figure 1). With increasing extrusion ratio, the texture becomes more intense so that some peaks disappear after the most heavy extrusion with $\varphi = 350$ (Figure 2(b)).

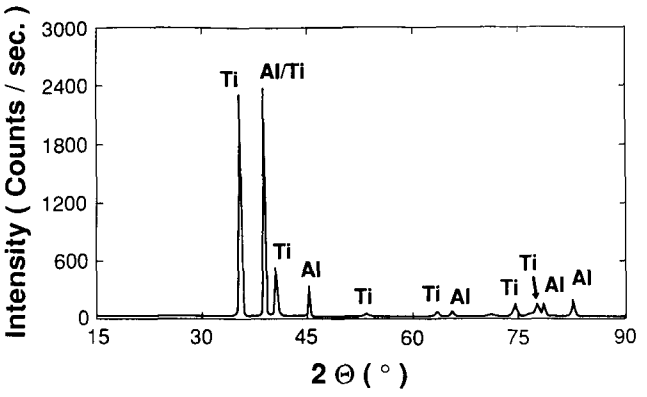

(*a*)

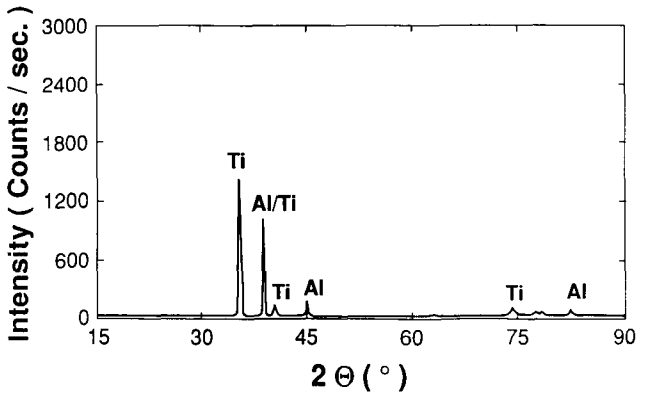

(*b*)

Fig. 2—X-ray diffraction diagrams of as-extruded conditions with extrusion ratio of (*a*) 17 and (*b*) 350.

B. *Pressureless Sinterings*

The previously mentioned three as-extruded specimens were pressureless sintered at 600 °C/6 h, 1000 °C/6 h, and 1350 °C/6 h. After these heat treatments, all three specimens are porous. Figure 3 shows LM photographs taken from specimens heat-treated at 1350 °C/6 h. The porosity is shown in Figure 4 as a function of temperature. It is obvious that the porosity decreases with increasing temperature. This is the case for specimens extruded with small extrusion ratios of 17 and 25. For example, the specimens with $\varphi = 17$ show a porosity of about 31.4 pct after sintering at 600 °C/6 h, much greater than after sintering at 1350 °C/6 h (15.9 pct). For the high extrusion ratio of 350, a porosity of 2.8 pct was measured after sintering at 600 °C/6 h, only a bit larger than the porosity after sintering at 1350 °C/6 h. The temperature effect by large extrusion ratio is not as large as that by small extrusion ratio. For a given sintering condition, the porosity decreases largely with increasing extrusion ratio. For specimens sintered at 1350 °C/6 h, the porosity was measured to be approximately 15.9 pct for $\varphi = 17$, 7.4 pct for $\varphi = 25$, and 2.0 pct for the high extrusion ratio of 350. At lower temperatures (600 °C/6 h and 1000 °C/6 h), larger porosities were obtained and the effect of extrusion ratio was also more pronounced.

Not only porosity but also pore size distribution is largely influenced by extrusion ratio (Figures 5 and 6). Defined as area on the specimen section, the pore size of almost all pores observed in the specimens with high extrusion ratio of 350 is smaller than 100 μm^2, whereas 45 to 60 pct of pores in specimens with low extrusion ratio of 17 are larger than 100 μm^2. For the extrusion ratio of 25, the fraction of pores larger than 100 μm^2 is about 28 to 36 pct. The largest pore after sintering at 600 °C/6 h has an area of about 3640 μm^2 for $\varphi = 350$, 9810 μm^2 for $\varphi = 25$, and 16,100 μm^2 for $\varphi = 17$. After sintering at 1350 °C/6 h, the largest pore was measured to be about 2130 μm^2 for $\varphi = 350$ and 9810 μm^2 for $\varphi = 25$ and $\varphi = 17$. The smallest pore sizes of about 4 μm^2 for $\varphi = 350$ and 16 μm^2 for $\varphi = 25$ and $\varphi = 17$ are given by the magnification factor used for pore area measurement, which was, due to much smaller pores, 200 for specimens with high extrusion ratio of 350, twice as large as for other specimens. For a given cumulative frequency, the pore size increases with decreasing extrusion ratio. For example, the pore size for the cumulative frequency of 50 pct, A_{50}, can be determined after sintering at 600 °C/6 h to be about 6 μm^2 for $\varphi = 350$, 28 μm^2 for $\varphi = 25$, and 200 μm^2 for $\varphi = 17$. After sintering at 1350 °C/6 h, A_{50} can be determined to be about 8 μm^2 for $\varphi = 350$, 60 μm^2 for $\varphi = 25$, and 80 μm^2 for $\varphi = 17$. The influence of sintering temperature increase on the pore size distribution seems not to be so clear (compare Figures 5 and 6). For the specimens with extrusion ratios of 25 and 350, the curve of cumulative frequency *vs* pore size is slightly shifted to larger pores. On the contrary, the curve for specimen of extrusion of 17 is shifted to smaller pores.

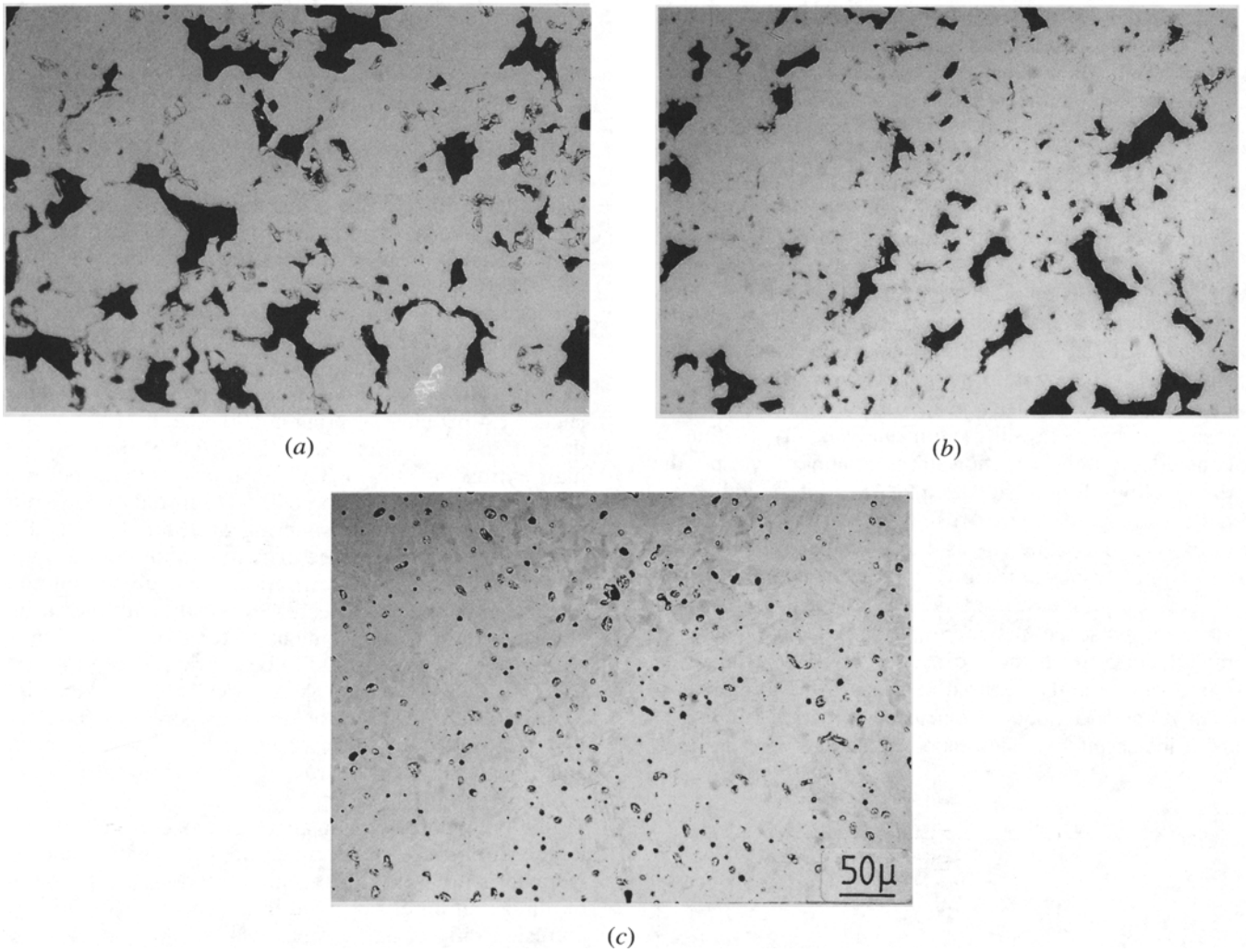

Fig. 3—LM photographs of specimens with extrusion ratio of (*a*) 17, (*b*) 25, and (*c*) 350 after pressureless sintering at 1350 °C/6 h; taken from specimen sections perpendicular to the extrusion direction.

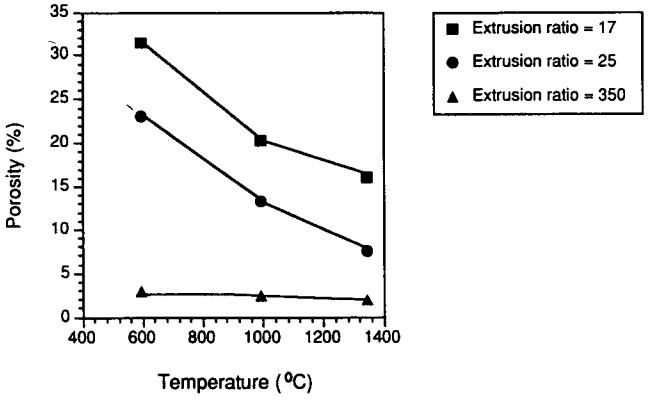

Fig. 4—Porosity of pressureless sintered specimens as function of temperature.

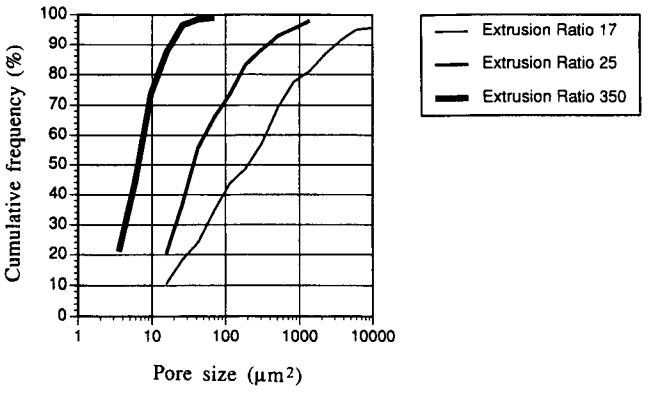

Fig. 5—Pore size distribution after pressureless sintering at 600 °C/6 h.

C. *HIP Treatment*

As mentioned in the introduction, a HIP treatment requires normal encapsulation of extruded pieces due to open porosity. Since encapsulation is normally very expensive, HIP without encapsulating is desirable in view of economy. We therefore attempted to carry out HIP treatment of the three as-extruded materials without encapsulation.

Figure 7 shows LM photographs of the three differently extruded specimens after the HIP treatment (1350 °C/4 h/200 MPa). These photos were taken in

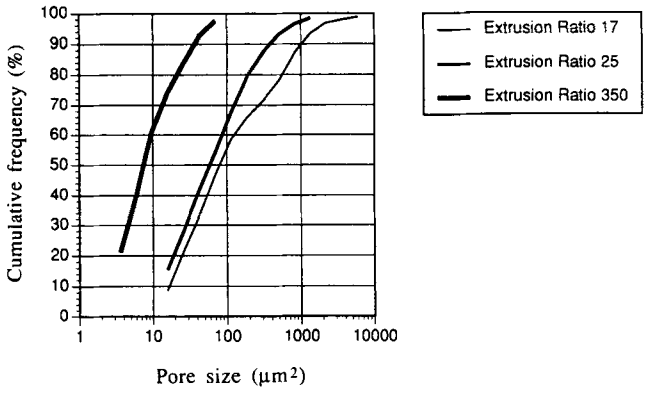

Fig. 6—Pore size distribution after pressureless sintering at 1350 °C/6 h.

the center of specimen sections. Near the surface of specimens with small extrusion ratios of 17 and 25, a small porosity is present (see, for example, Figure 8), whereas the specimen extruded with $\varphi = 350$ does not have such a clear zone of lower porosity. For the case of the small extrusion ratio, the pore size distributions near the surface and in the center of specimen differ from each other. Near the surface of the specimen, more small pores were seen, whereas the fraction of large pores became large in the center of the specimen (Figure 8(b)).The average porosity was measured to be 6.5 pct and 4.9 pct for specimens extruded with $\varphi = 17$ and $\varphi = 25$, respectively. They are much smaller than those after pressureless sintering at the same temperature (1350 °C/6 h). The reduction of porosity is doubtless due to the pressure applied for HIP treatment. However, this effect of pressure cannot be as clearly observed for the specimen extruded with the high extrusion ratio of 350. For this specimen, a porosity of 2.1 pct was measured, nearly the same as after the pressureless sintering at 1350 °C/6 h. The pore size distribution in the center of hot isostatically pressed specimens is shown in Figure 9. It can also be seen that the fraction of large pores increases with decreasing extrusion ratio. The fraction of pores larger than 100 μm^2 is smaller than 0.5 pct for $\varphi = 350$, about 16 pct for $\varphi = 25$, and 32 pct for $\varphi = 17$. The pore size for 50 pct cumulative frequency A_{50} is about 6 μm^2 for $\varphi = 350$, 22 μm^2 for φ

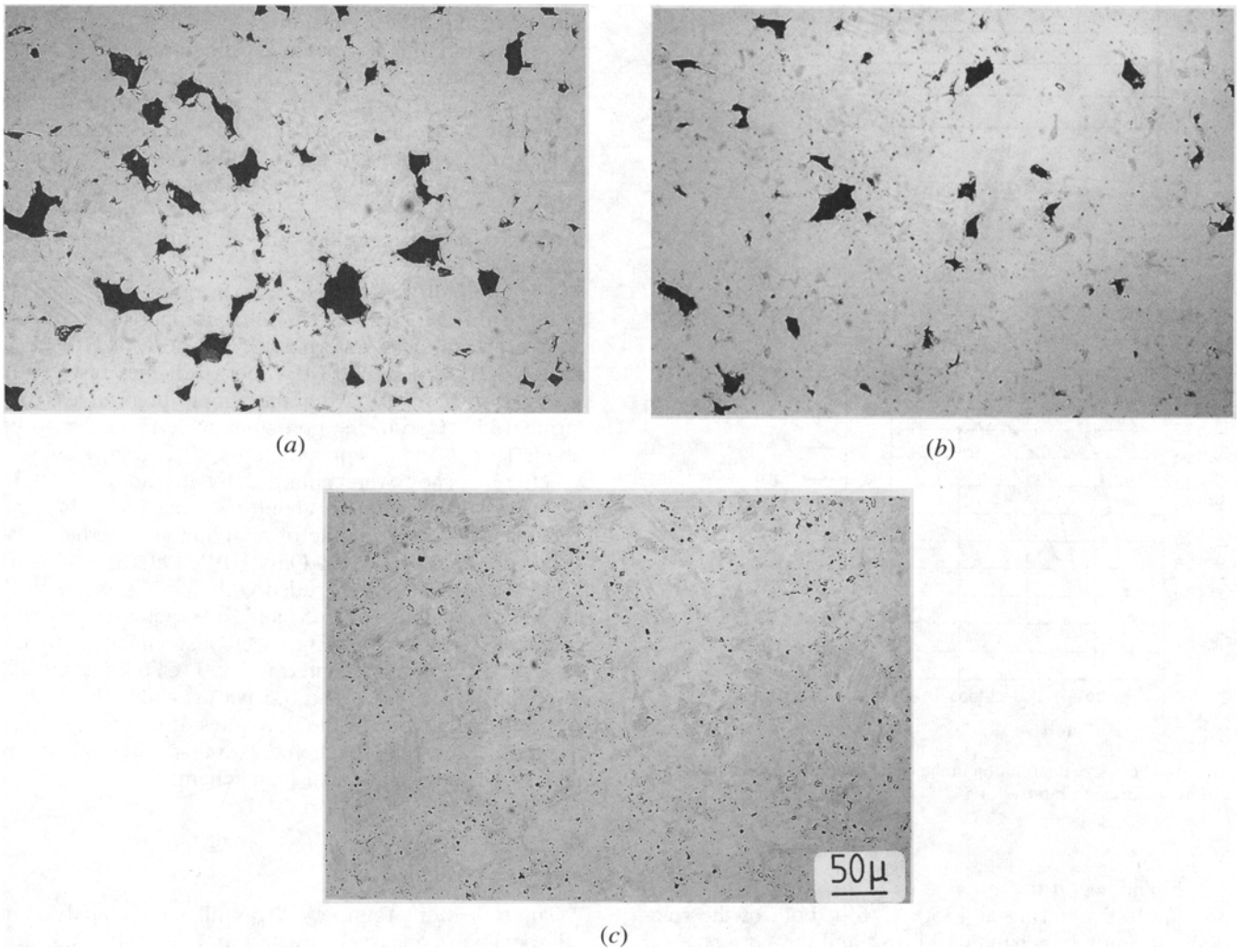

(a) (b) (c)

Fig. 7—LM photographs of specimens with extrusion ratio of (*a*) 17, (*b*) 25, and (*c*) 350 after HIP treatment at 1350 °C/4 h/200 MPa; taken from specimen sections perpendicular to the extrusion direction.

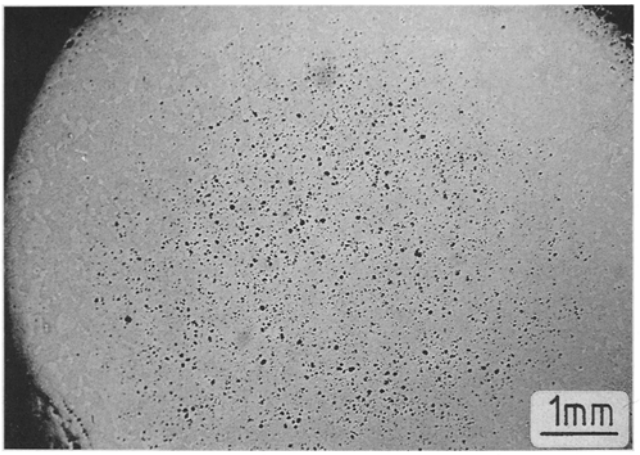

(*a*)

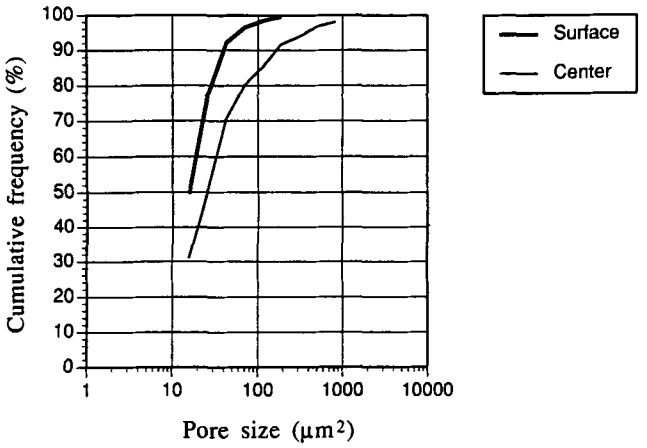

(*b*)

Fig. 8—(*a*) Different porosity and (*b*) pore size distribution in specimen extruded with extrusion ratio of 25 after HIP treatment 1350 °C/4 h/200 MPa.

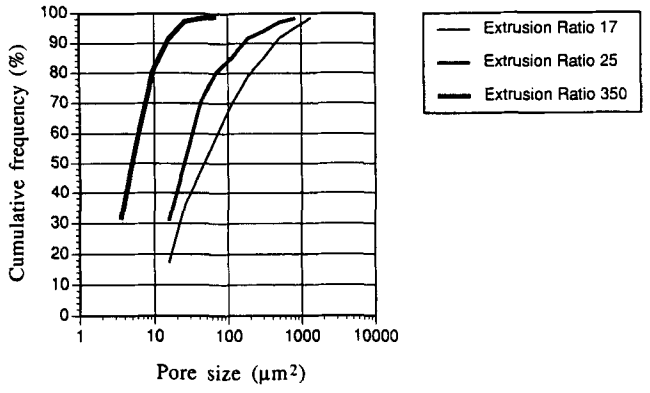

Fig. 9—Pore size distribution in the center of HIP'ed specimens with different extrusion ratios.

= 25 and 40 μm^2 for φ = 17. In comparison with pressureless sintering at 1350 °C/6 h, both of the fractions of pores larger than 100 μm^2 and the pore size for 50 pct cumulative frequency have been clearly reduced by applying pressure.

D. *Two-Step Sinterings*

Since the cost for HIP treatment increases with increasing HIP time, it is of practical importance to reduce the HIP time. However, this is limited because of the time required to complete the reaction between elemental Ti and Al to form the intermetallics TiAl and Ti_3Al. In addition, the process of pore shrinkage during HIP is also time dependent (creep process). In this respect, a two-step sintering, *i.e.*, a combination of the relatively cheaper pressureless sintering and the expensive HIP treatment, seems to be reasonable. In this work, two variations were carried out:

Scheme 1: pressureless sintering (1350 °C/6 h)
+ HIP (1350 °C/4 h/200 MPa)

Scheme 2: HIP (1350 °C/4 h/200 MPa)
+ pressureless sintering (1350 °C/6 h)

The porosities after these treatments are shown in Figure 10, together with those after the pressureless sintering 1350 °C/6 h (PS) and after the HIP treatment 1350 °C/4 h/200 MPa (HIP). It is visible that the treatment scheme does influence the final porosity and that this influence seems also to be dependent on extrusion ratio. For the high extrusion ratio of 350, scheme 1 is more beneficial than scheme 2. The porosity after treatment of scheme 1 is only 0.7 pct, much smaller that that for scheme 2 (5.0 pct). The pores formed during the pressureless sintering 1350 °C/6 h (Figure 3(c)) have been almost fully suppressed by the additional HIP treatment (Figure 11(a)). On the contrary, the relatively high-density HIP'ed material (Figure 7(c)) became more porous after the postpressureless sintering at 1350 °C/6 h (Figure 11(b)).

The situation for small extrusion ratios of 17 and 25 is quite different (Figure 10). In comparison with the simple pressureless sintering 1350 °C/6 h or HIP treatment 1350 °C/4 h/200 MPa, both schemes resulted in increase of porosity. After the simple pressureless sintering 1350 °C/6 h, the porosities were measured to be about 16 pct and 7.4 pct for φ = 17 and φ = 25, respectively. They were enlarged by the additional HIP treatment (scheme 1) to about 19.4 pct (φ = 17) and 12.3 pct (φ = 25) in spite of applying an external pressure as high as 200 MPa. Only HIP'ed at 1350 °C/4 h/200 MPa, specimens extruded with φ = 17 and φ = 25 showed porosities of 6.5 and 4.9 pct, respectively (Figures 7(a) and 7(b)). They were also enhanced by the following pressureless sintering 1350 °C/6 h (scheme 2) to about 9.1 (φ = 17) and 8.5 pct (φ = 25). For extrusion ratio of 17 or 25, the porosities after scheme 1 are larger than those after scheme 2 so that scheme 2 seems here to be more beneficial than scheme 1.

E. *X-ray Diffraction Analysis of Reactive Sintered Specimens*

The reflections found by X-ray diffraction analysis in all specimens reactively treated at $T \geq 1000$ °C, *i.e.*, specimens sintered at 1000 °C/6 h and 1350 °C/6 h, specimens HIP'ed at 1350 °C/4 h/200 MPa, as well as

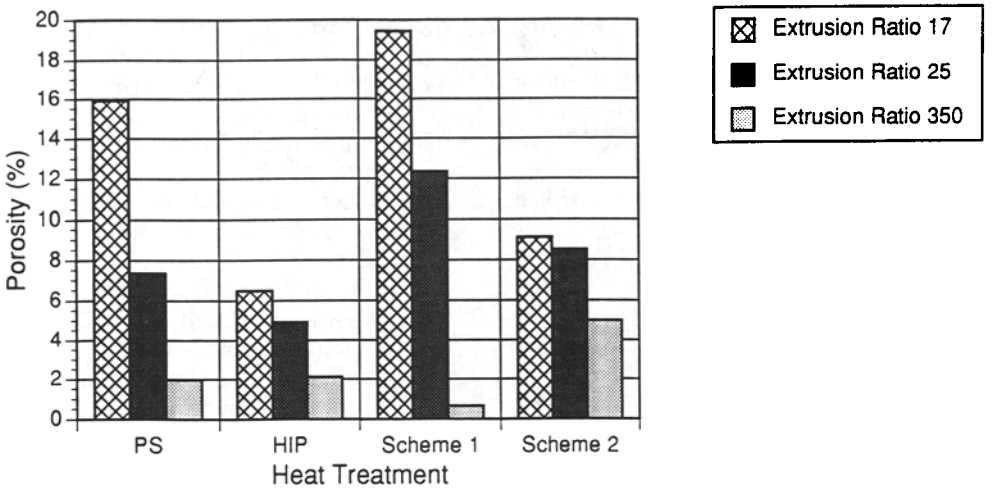

Fig. 10 — Porosity of specimens with different extrusion ratios as function of treatment.

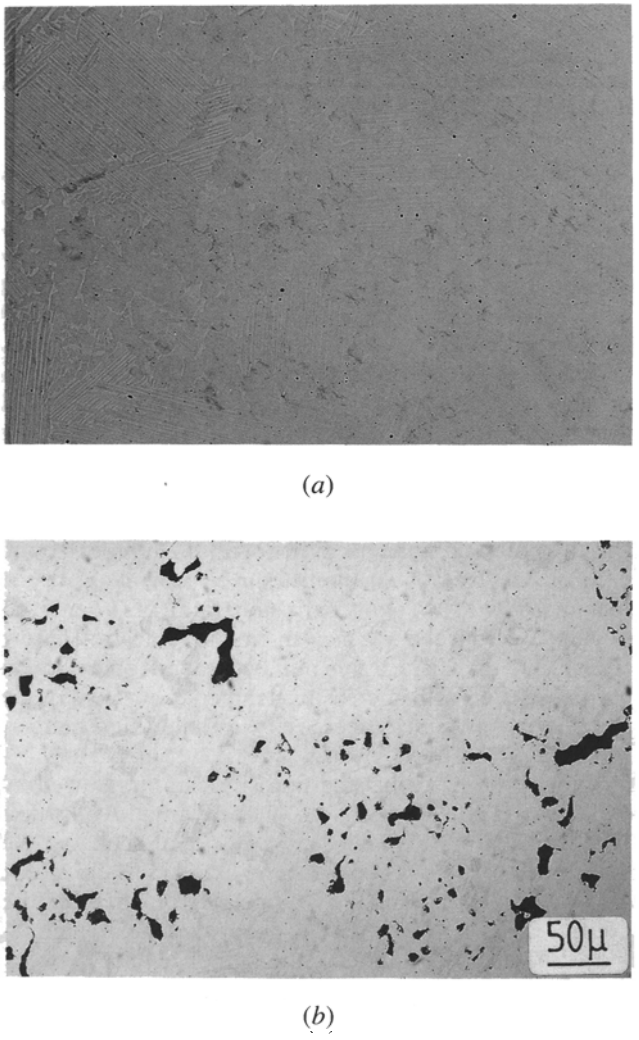

(*a*)

(*b*)

Fig. 11 — LM photographs of specimen extruded with extrusion ratio of 350 after combined treatments: (*a*) pressureless sintering 1350 °C/6 h followed by HIP 1350 °C/4 h/200 MPa and (*b*) HIP 1350 °C/4 h/200 MPa followed by pressureless sintering 1350 °C/6 h.

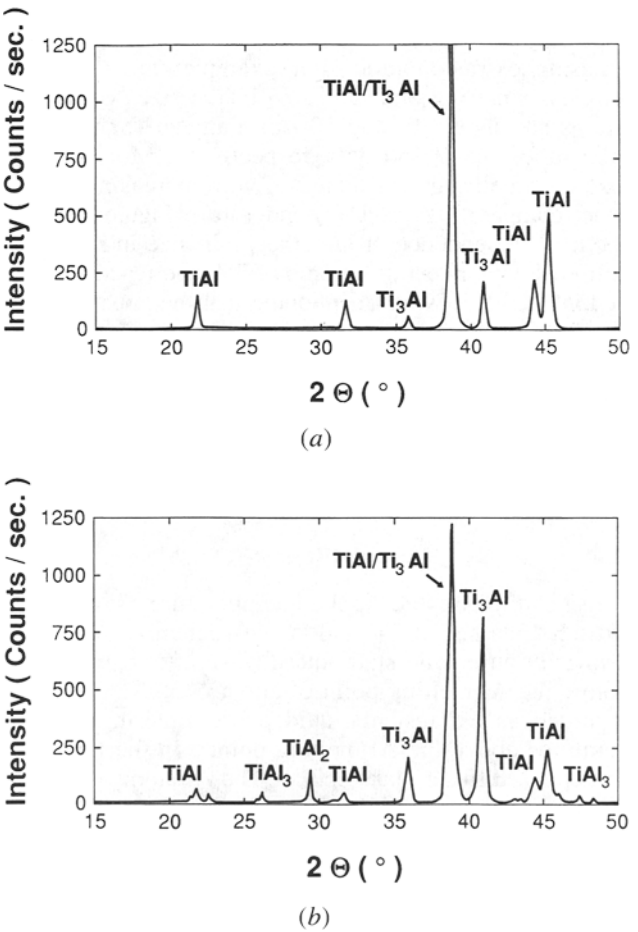

(*a*)

(*b*)

Fig. 12 — Typical X-ray diffraction diagrams of reactive treated specimens: (*a*) 1000 °C/6 h and φ = 17 and (*b*) 600 °C/6 h and φ = 17.

specimens treated after schemes 1 and 2, are identified as belonging to the intermetallic phases TiAl and Ti_3Al (Figure 12(a)). Only in the specimens sintered at 600 °C/6 h were additional reflections of the intermetallic phases $TiAl_3$ and $TiAl_2$ observed (Figure 12(b)). Both $TiAl_3$ and $TiAl_2$ are intermediate products of the reaction between Ti and Al. They will be consumed in progress of the reaction in favor of formation of the phases TiAl and Ti_3Al.[1,4] No peaks of pure Ti and Al were detected in any reactive sintered specimens.

F. *Microstructural Features*

Basically, all reactive treated specimens consist of two intermetallic phases, TiAl and Ti_3Al, as the results of X-ray diffraction analysis revealed. However, the morphology of both phases is dependent on the temperature applied for treatment. Depending upon the temperature applied for pressureless sintering or HIP, two types of microstructure were observed in this work. At 600 °C and 1000 °C, a dual-phase structure consisting of Ti_3Al islands in a matrix of equiaxed TiAl grains is developed (Figure 13(a)). For all specimens sintered or HIP'ed at 1350 °C, a typical duplex structure with TiAl and Ti_3Al lamellae and equiaxed TiAl regions is visible (Figures 3 and 13(b) and (c)). Both structures differ from each other in the hard dispersions which are the Ti_3Al islands in the dual-phase structure and the lamellar regions in the duplex structure. On the contrary, the matrix in both structures consists of the same TiAl phase. The grain size, especialy the size of lamellar grains, decreases with increasing extrusion ratio. For example, after the pressureless sintering at 1350 °C/6 h, the sizes of lamellar grains are about 70- and 50-μm diameter for the extrusion ratios of 17 and 350, respectively. Moreover, the size of lamellar grains increases with increasing treating time (compare Figures 13(b) and 13(c)). Figure 14 shows the time dependence of lamellar grain size in specimens extruded with an extrusion ratio of 350 and reactive treated at 1350 °C. It is worth mentioning that the lamellar grains in all specimens investigated in this study are much smaller than those of the alloys prepared by ingot metallurgy (larger than 300 μm; see, for example, Reference 5). Formation of dual-phase structure or duplex structure was the topic of an earlier article[2] and will not be treated here in detail.

IV. DISCUSSION

Depending on the applied temperature, sintering of extruded elemental Ti- and Al-powder mixtures can be primarily pure solid state interdiffusion (at temperatures below the Al melting point of about 655°C) or it can be regarded as a transient liquid phase sintering (at temperatures above the Al melting point). In the first case, Kirkendall diffusion takes place. The Al atoms move into Ti particles, whereas the Ti atoms stay almost immobile.[6] As a result of such one-sided diffusion, the originally dense specimens of the as-extruded conditions (Figure 15(a)) become porous, with pores being situated mostly at the interface region (Figure 15(b)). In the second case, Al melt flows away along particle or grain boundaries, leaving pores behind (Figure 15(c)). The Al melt then wets the Ti particles so that the contact surface between Ti and Al is enlarged and the reaction between Ti and Al is accelerated. The products of the reaction are the intermetallics, such as $TiAl_3$, $TiAl_2$ (as two intermediate products), TiAl, and Ti_3Al,[1,4] which are indicated by the hatched areas in Figure 15. After all elemental Al has been consumed, further solid state interdiffusion between Ti and the intermetallics formed can take place. The final microstructure consists of the intermetallics TiAl and Ti_3Al and pores (Figure 15(d)).

If sintering is carried out at temperatures lower than the Al melting point, such as pressureless sintering at 600 °C/6 h, then the situation in Figure 15(c) is absent. Kirkendall diffusion is responsible for the pore formation during this sintering. The conditions shown in Figure 15 can also appear successively during a sintering process. This is the case in pressureless sintering at 1000 °C/6 h or at 1350 °C/6 h. The Kirkendall diffusion (Figure 15(b)) took place during heating prior to the Al melting point. Because of the relatively high heating rate of 20 °C/min, the fraction of the porosity due to the Kirkendall diffusion must be considered to be not essential for both treatments. We can thus assume that the pore sizes immediately after the flow away of Al melt are approximately equal to the sizes of Al fibers of the as-extruded conditions; *i.e.*, the specimen with the high extrusion ratio of 350 has much smaller pores at this stage than those in the specimens with the low extrusion ratio of 17 or 25. Later, pore sizes as well as porosities will be reduced. This has been confirmed by the dilatometric measurement of Leitner *et al.*[7] They have shown that a volume reduction takes place after a maximum of dimensional increase has been reached. This volume reduction is observed at later stages of the sintering, at which no Al melt is present. It is thus believed that dislocation creep processes due to the well-known capillarity take place in the solid state and lead to the reduction of pore sizes as well as porosities. Under the action of the capillary forces, vacancy migration (Nabarro-Herring creep) and dislocation climb (Peach-Köhler creep) can take place. The capillary force increases with decreasing pore size.[8] Due to larger capillary forces, the pore size and the porosity in the specimen with the high extrusion ratio of 350 have been more reduced than those in the specimens with the low extrusion ratio of 17 and 25 (Figure 3). Both the vacancy migration (Nabarro-Herring creep) and the dislocation climb (Peach-Köhler creep) become easier with increasing temperature. Hence, the porosity and pore size decrease with increasing temperature (Figures 4 through 6).

Shibue[9] showed that the porosity can be reduced by replacing Al powder with Al-7 wt pct Mn alloy powder. This can also be explained as a result of reducing the size of the Al fibers. For the same extrusion ratio of 15, the as-extruded Ti- and Al-7 wt pct Mn powder mixture exhibits a finer microstructure than the as-extruded Ti- and Al-powder mixture. The strength difference between Ti and Al is reduced by using the Mn alloyed Al powder so that Ti particles are more deformed during extrusion. For a constant section area of extruded parts, *i.e.*, for a same extrusion ratio, this means a reduction of both Ti and Al fibers.

Both vacancy migration and dislocation climb can be

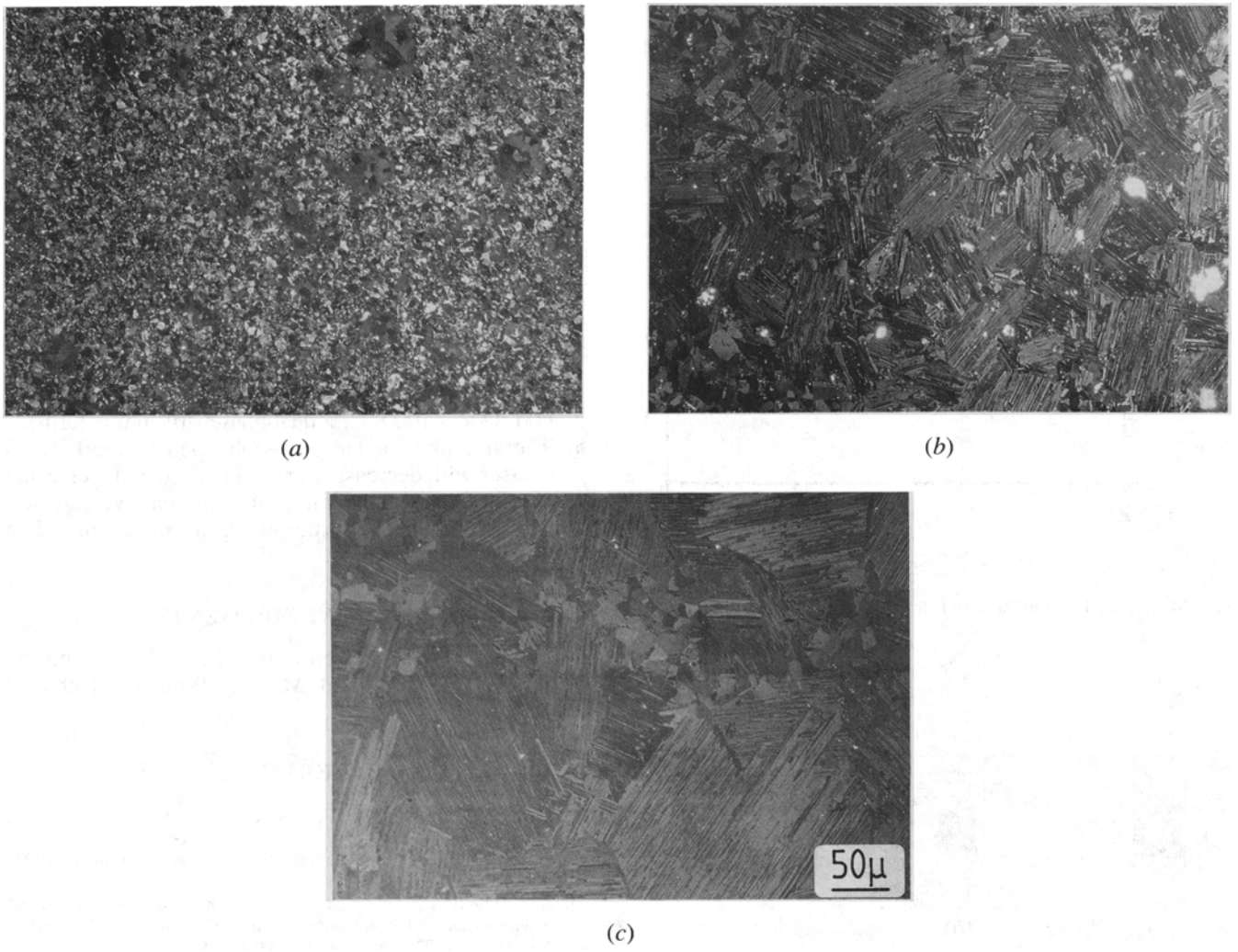

Fig. 13—Polarized LM photographs of specimens extruded with extrusion ratio of 350 showing (*a*) dual-phase structure developed at 1000 °C/6 h, (*b*) duplex structure developed after pressureless sintering at 1350 °C/6 h, and (*c*) after combined treatments: 1350 °C/6 h + 1350 °C/6 h/200 MPa.

accelerated by applying an external pressure resulting in a reduction of porosity, provided that no gas from the environment penetrates into the specimens. If as-extruded materials which are nearly pore-free (Figure 1) are directly HIP'ed, then gas penetration is limited, at least at the beginning of the HIP treatment. This can be the reason for the relatively lower porosities of simple HIP'ed specimens, especially near the specimen surface (Figures 7 and 8). Experimental results of pressureless sinterings show that the overall porosity can be greatly reduced by applying a high extrusion ratio. Open porosity after pressureless sintering must also be decreased with increasing extrusion ratio. Gas penetration must therefore be largely limited for specimens extruded with high extrusion ratio of 350 so that very low porosities have been obtained through pressureless sintering followed by HIP treatment (Figures 10 and 11(a)). On the contrary, gas penetration can easily take place in specimens extruded with low extrusion ratios of 17 and 25, which are very porous after pressureless sintering (Figures 3(a) and (b)). This accounts for the high porosities of these specimens after treatments of scheme 1, *i.e.*, first pressureless sintering and then HIP treatment (Figure 10).

The vacancy migration can also introduce Ostwald ripening, during which small pores are consumed to form large pores. For a given detection limit, the measured porosity will be larger due to Ostwald ripening, although the real porosity should not be changed by Ostwald ripening. Moreover, swelling of the gas included in specimens at HIP treatment can also cause an increase of porosity. Taking these two factors into account, it is easy to understand why porosities of HIP'ed specimens were increased by additional pressureless sintering (Figures 7, 10, and 11(b)).

V. CONCLUSIONS

The results obtained in this study can be summarized as follows.

1. For pressureless sintering, the maximum pore size as well as the porosity can be effectively reduced by applying a high extrusion ratio. This effect is larger at higher temperatures.

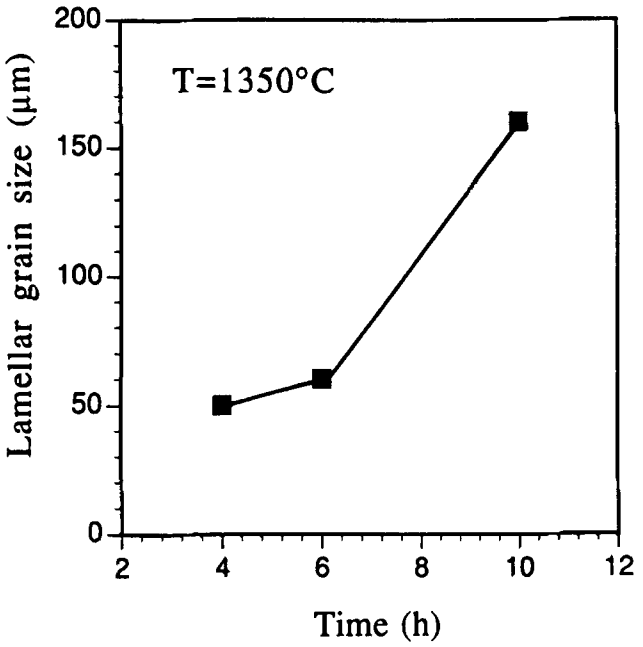

Fig. 14—Lamellar grain size at 1350 °C as function of time.

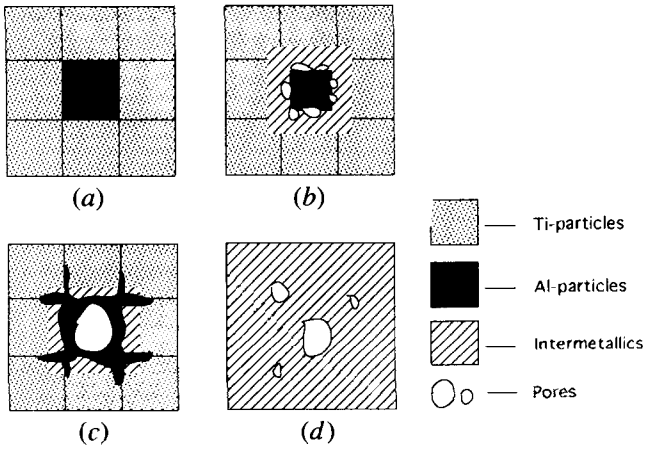

Fig. 15—Schematic description of reaction sintering process of extruded Ti- and Al-powder mixtures: (*a*) as-extruded condition; (*b*) after certain Kirkendall diffusion; (*c*) after flow away of Al melt; and (*d*) after complete reaction sintering.[10].

2. By applying a high extrusion ratio, it is possible to prepare nearly pore-free material by HIP treatment without encapsulating.
3. To reduce expensive HIP time, a combination of pressureless sintering and HIP can be applied. Whether HIP should be carried out before or after pressureless sintering depends on the extrusion ratio applied. For extrusion ratio as high as 350, it is more beneficial with respect to porosity to carry out HIP after prior pressureless sintering than the reverse route. For low extrusion ratio, HIP should be performed before pressureless sintering.
4. Depending on the temperature applied, different types of microstructures can be obtained. In this work, a duplex structure is developed at 1350 °C, whereas at 600 °C and 1000 °C, a dual-phase structure is formed.
5. The size of lamellar grains obtained at 1350 °C increases with decreasing extrusion ratio and increasing treating time. Lamellar grains of reactive powder-processed material in this work are much finer than those of ingot alloys.

ACKNOWLEDGMENTS

The authors would like to thank Ms. W.-V. Schmitz, Ms. B. Wildhagen, and Mr. K. Wulf for technical assistance.

REFERENCES

1. G.-X. Wang and M. Dahms: *Powder Metall. Int.*, 1992, vol. 24 (4), pp. 219-25.
2. G.-X. Wang and M. Dahms: *Scripta Metall. Mater.*, 1992, vol. 26 (5), pp. 712-22.
3. K.B. Mueller, X. Neubert, and M. Dahms: in J.M. Capus and R.M. German, eds., *Advances in Powder Metallurgy & Particulate Materials—1992*, Princeton, NJ, MPIF, 1992, vol. 7, pp. 139-53.
4. G.-X. Wang, U. Bohnenkamp, and M. Dahms: *Proc. Metallographietagung*, Dresden, Sept. 30–Oct. 2, 1992, in press.
5. Y.-W. Kim and D. M. Dimiduk: *JOM*, 1991, Aug. pp. 40-47.
6. F.J.J. van Loo and G.D. Rieck: *Acta Metall.*, 1973, vol. 21, pp. 61-71.
7. G. Leitner, M. Dahms, and S. Schultrich: *Proc. 8th Int. Conf. on Powder Metallurgy in CSFR*, Pistany, CSFR, Oct. 7–9, A. Salak and M. Selecka, eds., 1992, vol. 2, pp. 243-52.
8. W. Schatt: *Pulvermetallurgie Sinter- und Verbundwerkstoffe*, VEB Deutscher Verlag für Grundstoffindustrie, Leipzig, 1984.
9. K. Shibue: *Sumitomo Light Met. Tech. Rep.*, 1991, vol. 32 (2), pp. 95-101.
10. G.-X. Wang and M. Dahms: *Scripta Metall. Mater.*, 1992, vol. 26 (9), pp. 1469-74.